ACS OMEGA

http://pubs.acs.org/journal/acsodf

Article

Hydroxyapatite Derived from Salmon Bone As Green Ecoefficient Support for Ceria-Doped Nickel Catalyst for CO_2 Methanation

Thi Thuy Van Nguyen, Nguyen Phung Anh, Thanh Gia-Thien Ho, Thi Thuy Phuong Pham, Phuc Hoang Duy Nguyen, Ba Long Do, Ha Ky Phuong Huynh,* and Tri Nguyen*

Cite This: *ACS Omega* 2022, 7, 36623−36633

Read Online

ACCESS | Metrics & More | Article Recommendations

ABSTRACT: Hydroxyapatite (HA) derived from salmon bone byproducts is used as a green support for the nanostructured nickel catalysts applied in the methanation of carbon dioxide (CO_2). Undoped nickel catalysts and various ceria-doped nickel supported on hydroxyapatite (HA) were prepared by coimpregnation. Characteristics of the as-prepared catalysts were investigated by the various techniques, including X-ray diffraction (XRD), scanning electron microscopy (SEM), Brunauer−Emmett−Teller (BET), hydrogen temperature-programmed reduction (H_2-TPR), carbon dioxide temperature-programmed desorption (CO_2-TPD), and energy-dispersive X-ray spectroscopy (EDX). The catalyst activity was assessed throughout CO_2 methanation in the low-temperature range of 225−350 °C with the molar ratio of H_2/CO_2 = 4/1. The function of HA and ceria provided a high dispersity of nickel particles over the catalyst surface with the size range of 24.5−25.8 nm, leading to improvement in the reduction and CO_2 adsorption capacity of the catalysts as well as enhancing the catalytic efficiency in CO_2 methanation. The 10Ni/HA catalyst reduced at suitable conditions of 400 °C for 2 h showed the highest catalytic performance among the tested catalysts. CO_2 conversion and CH_4 selectivity reached 76.6 and 100% at a reaction temperature of 350 °C, respectively. The results show that the Ni/HA sample doped with 6.0 wt % ceria was the best, with the CO_2 conversion and the CH_4 selectivity reaching 92.5% and 100%, respectively, at a reaction temperature of 325 °C.

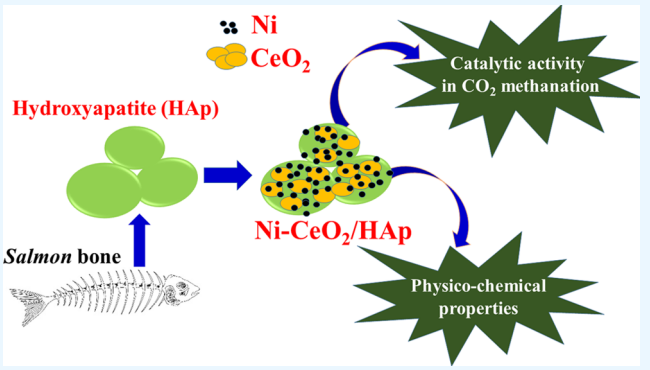

1. INTRODUCTION

The global population explosion has led to a continuous increase in energy demand. According to the U.S. Energy Information Administration,[1] world energy consumption is projected to rise by 28% between 2015 and 2040. Most of the world's energy comes from fossil fuels, including oil and coal. The burning of these fuels has caused global warming, which leads to climate change due to ever-increasing levels of CO_2 in the atmosphere.[2−4] Global CO_2 emissions from fossil fuel combustion and other processes are estimated to be 35.7 billion tonnes annually.[5] The ambient air concentration of CO_2 in the atmosphere has surpassed 400 ppm from 316 ppm in 1958, with an average global temperature before the industrial revolution by 1.5 °C. Average global CO_2 concentration is expected to keep rising and exacerbate climate change that adversely impacts global populations.

Despite considerable efforts in creating and developing new clean energy sources, fossil fuels still account for nearly 80% of total global energy consumption.[6] Therefore, it is required to develop clean technologies using fossil fuels as well as to produce renewable and environmentally friendly energy sources to mitigate the negative impacts of climate change. The approach to reduce CO_2 emission is to substitute coal and fossil fuel by natural gas, which consist mainly of methane, as natural gas emits about half the amount of carbon dioxide than coal for the same energy produced due to the lower carbon content and more efficient combustion of natural gas.[7] However, natural gas is a nonrenewable energy source. Thus, methane production via CO_2 hydrogenation has drawn attention.

CH_4 is an energy-rich carrier that can be stored in the liquified form under the cryogenic condition with current infrastructure and facilities. Sustainable methane production on a commercial scale while reducing CO_2 emissions may help to ensure energy security.[8] Chemically, CO_2 is an inert and

Received: July 21, 2022
Accepted: September 29, 2022
Published: October 5, 2022

ACS Publications

© 2022 The Authors. Published by American Chemical Society

inactive gas, so the CO_2 methanation requires the addition of catalysts to enhance the reaction efficiency. The most thoroughly researched metal is nickel (Ni) due to its relatively high activity, exceptional CH_4 selectivity, and lower cost compared to noble metals.[9−11] Precious metals such as Rh, Ru, Pd, etc., show higher activity than Ni, but they are not widely used because of their limited availability and high price. Metal oxides such as γ-Al_2O_3, SiO_2, TiO_2, CeO_2, SBA-15, etc., are the most used supports for Ni catalysts for CO_2 hydrogenation.[12] However, they have certain disadvantages, such as easy deactivation promoted by carbon deposition and metal loss, leading to lower activity and selectivity, as well as the ability of coke formation.[12] Furthermore, their scarcity and high cost limit their utility in supporting this process. Therefore, the enhancement of the catalytic activity as well as stability of nickel catalysts by changing or improving the supports remains a significant challenge.

Thus, it is desirable to expand our perspective to another type of catalyst support. In recent years, hydroxyapatite (HA) has been promoted as an alternative and sustainable source of catalyst support as it is a common component found in bones.[13] The crystal lattice structure of $Ca_{10}(PO_4)_6(OH)_2$ is arranged in a hexagonal shape including Ca^{2+}, PO_4^{3-}, OH^- ions in space group $P63/m$ with crystal parameters at a = 9.418 Å, c = 6.881 Å, β = 120°.[14] Therefore, the active phases can be immobilized on the HA surface thanks to the ion exchange capacity of HA.[15] Ca^{2+} cations on the HA surface are reported to adsorb molecular CO_2 to the surface even at room temperature.[16] In addition, the weak base property of HA can limit the side effects caused by the support itself. This property can be controlled by regulating Ca/P. Thanks to the OH^- group rich surface, HA can prevent the Ni catalyst from being poisoned by CO, stabilize the active phases, and prevent their aggregation.[17,18] Furthermore, because HA has a high thermal stability and is only structurally altered at temperatures above 1000 °C, the sintering of NiO species can be significantly reduced. The weakly basic nature of the HA surface and high thermal stability have been utilized and reported for various high-temperature catalytic reactions, including the oxidative coupling of methane,[19] the oxidative dehydrogenation of propane,[20] the dry reforming of methane,[21] the water gas shift reaction,[22] and CO oxidation.[23] However, few studies have been conducted on the possibility of using HA as a potential support for CO_2 methanation.

The presence of additives also significantly improves the catalytic activity and stability in the methanation reaction. Recently, studies have found that ceria (CeO_2) is an additive capable of forming base centers that effectively promote the adsorption and activation of CO_2 molecules on the catalyst.[24] Because of its high oxygen storage and transport capacity, CeO_2 can release oxygen in oxygen-poor environments and rapidly reoxidize under oxygen-rich environments.[25] In redox reactions, ceria plays an essential role in delivering lattice-derived oxygen and substitution through the dissociation of carbon dioxide on the surface.[26−28] Li et al.[29] also demonstrated that the addition of CeO_2 improves the interaction between the support and the active metal phase, allowing better control of the Ni particle dispersion, thus enhancing the performance of Ni-based catalysts. According to research by Xavier et al.,[30] the addition of CeO_2 could decrease the reduction temperature of β-NiO and change the fractions of NiO species on the Ni/Al_2O_3 catalyst surface. This showed that CeO_2 reduced the strong interaction between Ni and Al, improving the reduction of Ni^{2+} to Ni^0. This positive effect is explained by the fact that CeO_2 reduces the bonding force between Ni metal and the support, thereby enhancing the reducing ability as well as the dispersion of Ni active sites on the support. Therefore, adding CeO_2 to the Ni/HA catalyst has the potential to boost the catalytic activity and stability.

In this study, nickel-based catalysts doped and undoped with various NiO and CeO_2 contents supported on HA derived from salmon bone byproducts were synthesized by impregnation method. The physicochemical properties of the as-prepared catalysts were characterized by several techniques and evaluated for their activity in CO_2 methanation.

2. EXPERIMENTAL SECTION

Catalyst Preparation. Hydroxyapatite (HA) was synthesized by the hydrothermal method from powder salmon bones that are discarded after enzymatic hydrolysis to obtain proteins. The powder-dried fish bones meal contains 72.4 wt % Ca, 23.1 wt % P, and 4.5 wt % other ingredients such as Mg, Si, S, etc. The molar ratio of Ca/P in the raw material is 2.41. To achieve the ideal Ca/P ratio value in HA (1.67), we added a small amount of P from the H_3PO_4 source in the HA synthesis. The HA preparation procedure was carried out according to the identified suitable one detailed in our previous study.[31] One gram of dried salmon bone powder (d < 0.10 mm) was dispersed in 50 mL of distilled water at room temperature and stirred at 300 rpm for 30 min. Then, a 1% H_3PO_4 solution (Xilong) was continuously added dropwise into the reaction mixture, and the 5% NH_4OH solution (Xilong) was used to maintain the pH at 10 during the synthesis duration. After another 2 h of stirring, the sol mixture was transferred to a Teflon autoclave for hydrothermal treatment at 120 °C for 7 h. After that, the resulting precipitate was separated by centrifuging at a speed of 5000 rpm for 30 min and washed with distilled water several times until the pH reached 7. The collected precipitate was dried at 80 °C for 24 h and finally calcined at 800 °C for 1 h in airflow with a ramping rate of 10 °C/min to obtain HA.

Nickel and ceria-doped nickel catalysts were loaded on HA by the impregnation method of $Ni(NO_3)_2{\cdot}6H_2O$ (≥99.9%, Prolabo) and $Ce(NO_3)_3{\cdot}6H_2O$ (≥99,9%, Merck) solutions. The obtained suspension was left to stand overnight before being dried in the air at 80, 100, and 120 °C within 2 h at each temperature, and then calcined in the air at 600 °C for 4 h with a ramping rate of 10 °C/min to obtain catalysts. The prepared Ni and CeO_2-doped Ni catalysts supported on HA were denoted as xNiyCe/HA, where x represented the weight percent of Ni in the catalysts, x = 5, 10, and 15; y illustrated the weight percent of CeO_2, y = 4, 6, and 8.

Catalyst Characterization. The physical-chemical characteristics of the obtained samples were studied by several methods, including X-ray diffraction on a Bruker D2 Phaser X-ray diffractometer with Cu Kα radiation and recorded in 2θ = 10−80° using the step scan mode with a step size of 0.03°; EDX spectrum on a JEOL JST-IT 200 instrument; nitrogen adsorption−desorption isotherms at −196 °C on a Nova 2200e instrument with the sample pretreated in a 30 mL/min nitrogen flow at 300 °C for 2 h; field-emission scanning electron microscopy on Hitachi S4800 instrument, hydrogen temperature-programmed reduction (H_2-TPR) carried out on a microreactor in a gas mixture of 10% H_2/N_2 at a flow rate of 30 mL/min using a gas chromatograph GOW-MAC 69−350 with a TCD detector and the used sample of 50 mg; and CO_2-

https://doi.org/10.1021/acsomega.2c04621
ACS Omega 2022, 7, 36623−36633

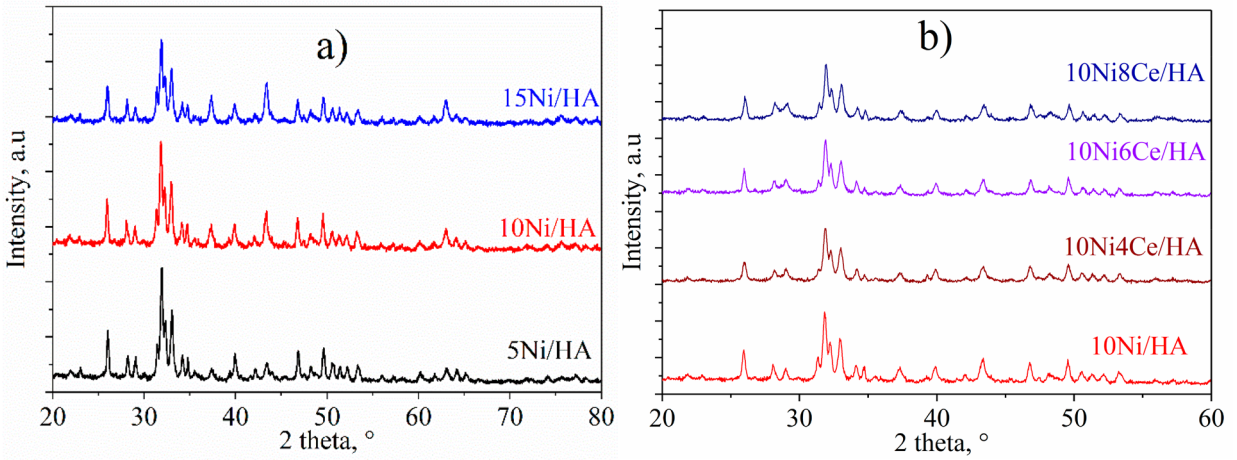

Figure 1. XRD patterns of Ni/HA catalysts of (a) undoped and (b) doped CeO_2.

programmed temperature desorption (CO_2-TPD) also carried out on a microreactor in He at a flow rate of 30 mL/min from 50 to 800 °C at a ramping rate of 10 °C/min in the above-mentioned gas chromatograph 350 instrument system with 100 mg of catalyst adopted in a quartz reactor and reduced at 450 °C for 1 h in pure H_2 at a flow rate of 30 mL/min prior to being cooled down to 50 °C.

Catalyst Performance Evaluation. The activity of the catalysts in CO_2 methanation was tested in a microflow reactor under atmospheric pressure at 225−400 °C with a CO_2/H_2 ratio of 1/4, feed flow rate of 3 L/h, and used catalyst mass of 0.2 g. Before conducting the reaction, the catalyst was reduced in the H_2 stream with the flow rate of 2 L/h at various temperatures (T = 400 and 450 °C with at a ramping rate of 10 °C/min) and durations (t = 1.5, 2.0, and 2.5 h). The reaction mixture was analyzed on an Agilent 6890 Plus gas chromatograph (HP-USA) using a thermal conductivity detector (TCD) (capillary column HP-PLOT MoleSieve 5A, 30 m length, 0.32 mm outer diameter, 0.25 μm thickness) and a flame ionization detector (FID) (capillary column DB624, 30 m length, 0.32 mm outer diameter, 0.25 μm thickness).

3. RESULTS AND DISUSSION

3.1. Properties of Studied Catalysts. XRD patterns of Ni/HA catalysts (Figure 1a) show characteristic diffraction peaks of HA with hexagonal structure at 2θ = 25.9, 27.8, 28.7, 31.8°, 32.0, 32.9, 34.0, 46.8, 49.5, 50.5, 51.3, 52.0, and 53.0° (JCPDS card No. 09−432). Besides the characteristic diffraction peaks of HA, the diffraction peaks of the β-TCP $Ca_3(PO_{4)2}$ phase were also detected at 2θ = 31.2, 34.7, and 42.1° (JCPDS card No. 09−169) with low intensity, indicating that a small amount of β−TCP $Ca_3(PO_4)_2$ was formed during HA modulation. According to Taimai et al.,[32] the Ca/P mole ratio, which was less than 1.8, caused HA to lack the Ca component (Ca-dHAP), leading to easy breakdown into HA and β-TCP. The decomposition of Ca-dHA at a calcination temperature of 800 °C was as follows:

$$Ca_{10-x}(HPO_4)_x(PO_4)_{6-x}(OH)_{2-x} \rightarrow Ca_{10}(PO_4)_6(OH)_2 + \beta\text{-}Ca_3(PO_4)_2 + xH_2O$$

The presence of β-TCP $Ca_3(PO_4)_2$ was also related to the pH of the reaction. Due to the synthesis of HA at pH < 10, besides the main product, HA, β-TCP wwas also discovered in trace form, as concluded by Huang et al.[33] The XRD spectrum also observed diffraction peaks of NiO at 2θ = 36.9, 43.3, 62.3, 74.7, and 78.6° (JCPDS card No.47−1049) with high crystallinity. Meanwhile, for Ce-modified 10Ni/HA samples, there is almost no appearance of the characteristic peaks of CeO_2 at 2θ = 28.2, 32.7, 47, 55.7, 58.5, 68.7, and 75.8° despite the CeO_2 load up to 8.0 wt % (Figure 1b). This proves that CeO_2 is in fine form and well dispersed on the HA surface. Research of Hu et al.[33] also gave similar results. Based on the XRD spectrum at 2θ = 43.3° (the highest intensity peak of NiO), the average crystal size of NiO was calculated based on the Scherrer equation and shown in Figure 2. It can be seen

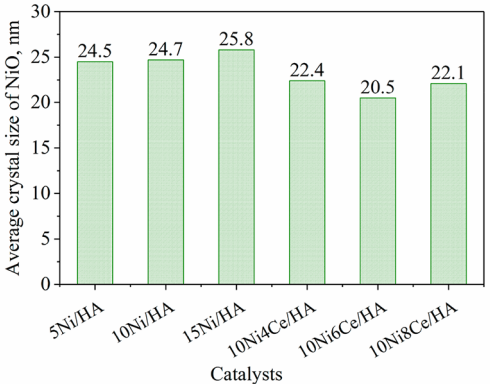

Figure 2. Average size of NiO crystal on the surface of catalysts.

that increasing NiO loading increases the crystal size due to the particle agglomeration under high NiO loading; however, the difference in NiO crystal size between samples 5Ni/HA and 10Ni/HA is insignificant, showing that agglomeration is almost less likely for the 10Ni/HA sample compared with the 15Ni/HA sample (the NiO crystal size is much larger than the 5Ni/HA and 10Ni/HA samples). Meanwhile, for the Ce-modified Ni/HA samples, the addition of ceria decreases the NiO crystal size by enhancing NiO dispersion on the HA surface, with the 10Ni6Ce/HA sample having the smallest size compared to others.

The elemental compositions of the 10Ni/HA and 10Ni6Ce/HA samples were determined by EDS analysis (Figure 3). The EDS spectrum of the 10Ni/HA sample showed the characteristic peaks of O, P, Ca, and Ni, with the mass ratio

https://doi.org/10.1021/acsomega.2c04621
ACS Omega 2022, 7, 36623−36633

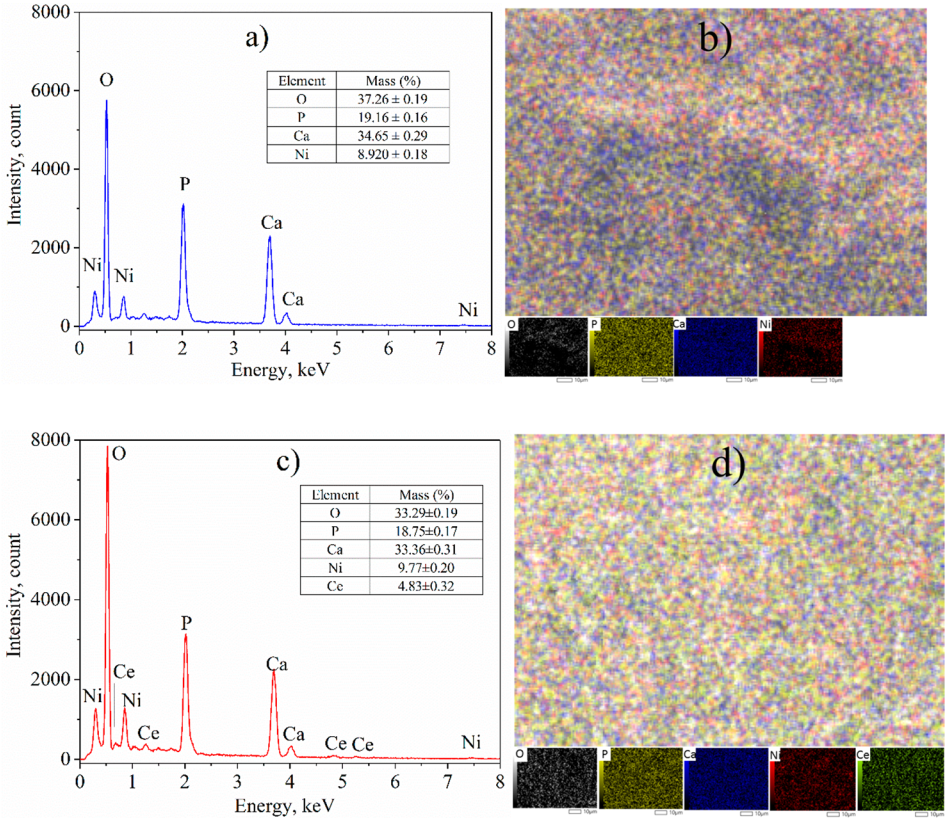

Figure 3. EDS spectra and element mapping of catalysts; (a, b) 10Ni/HA and (c, d) 10Ni6Ce/HA.

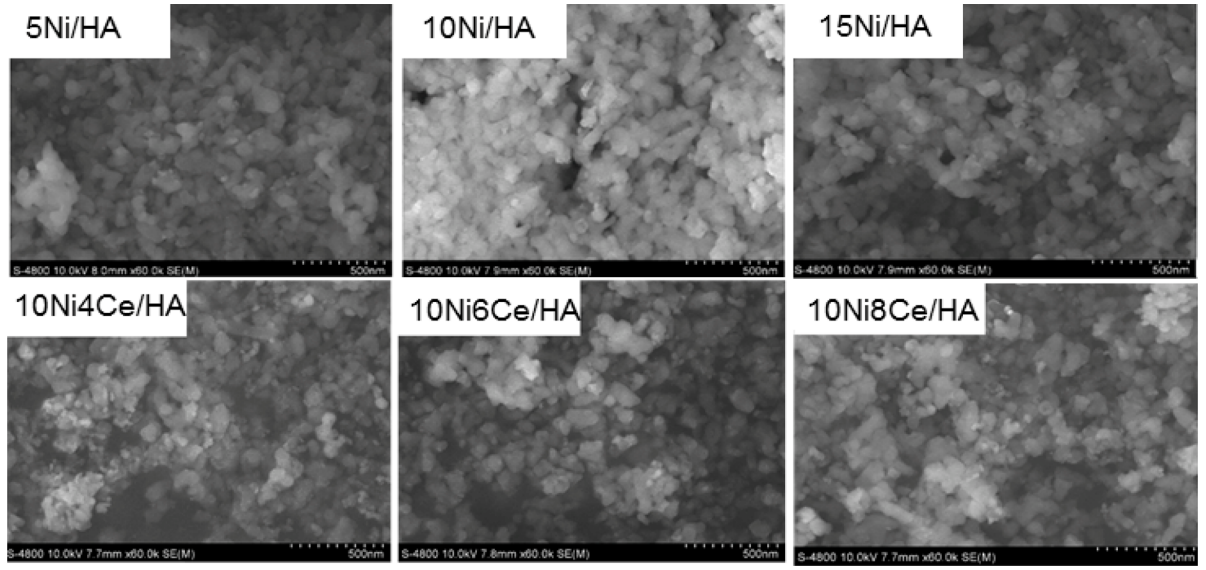

Figure 4. SEM images of as-prepared catalysts.

corresponding to 37.26:19.16:34.65:8.92. Similarly, the EDS spectrum of the 10Ni6Ce/HA sample also shows characteristic peaks of O, P, Ca, Ni, and Ce with a mass ratio of 33.29:18.75:33.36:9.77:4.83 (Figure 3a, c). These ratios are also relatively close to the theoretical mass ratios excluding the hydrogen component of samples (10Ni/HA 39.22:16.44:35.45:8.89; 10Ni6Ce/HA 37.39:15.35:33.11:8.89:5.26). The Ca/P ratios of 10Ni/HA and 10Ni6Ce/HA samples were obtained at 1.79 and 1.69, respectively. This is entirely consistent with Tamai in the case of samples with the presence of β-TCP $Ca_3(PO_4)_2$ phase with a Ca/P ratio <1.8.[32] On the HA support, the elements of the active phase and the doping are fairly uniformly distributed. Compared with the pure Ni/HA catalyst, the ceria-modified one has a more uniformly dispersed Ni phase composition on the surface (Figure 3b, d). Besides, from the EDS and XRD results, it can be concluded that the nickel and ceria phases formed and uniformly dispersed on the surface as well as inside the structure of HA.

https://doi.org/10.1021/acsomega.2c04621
ACS Omega 2022, 7, 36623−36633

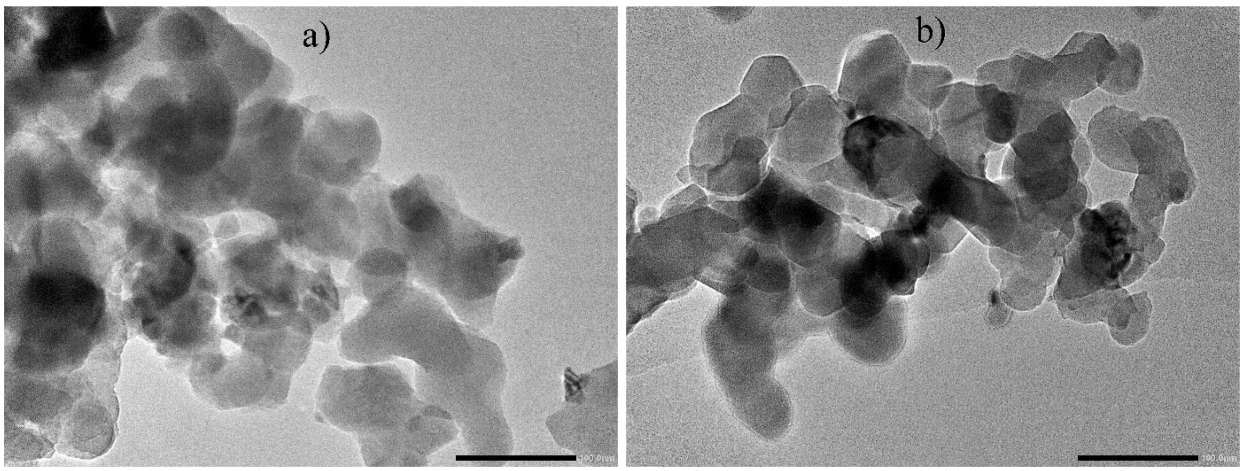

Figure 5. TEM images of as-prepared catalysts: (a) 10Ni/HA and (b) 10Ni6Ce/HA.

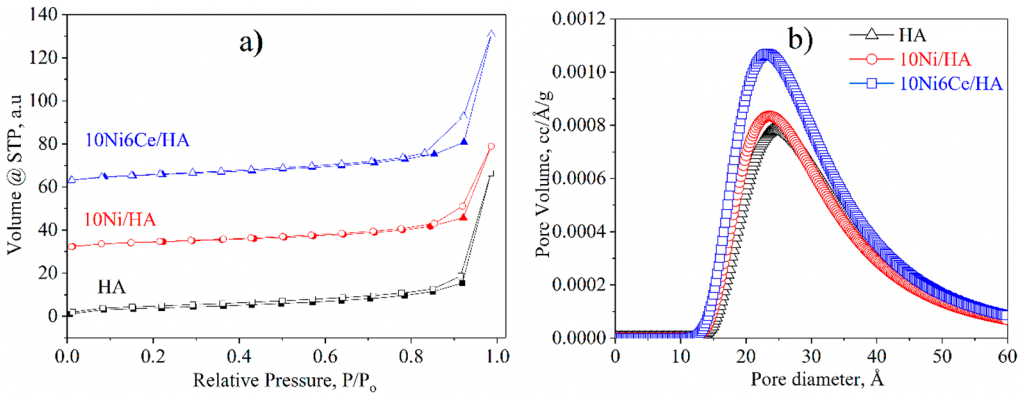

Figure 6. (a) N_2 adsorption/desorption isotherm and (b) BJH pore diameter distribution of catalysts.

SEM images of the catalysts (Figure 4) show small NiO metal particles (15−30 nm) distributed relatively uniformly on the HA surface with a spherical shape. For the unmodified CeO_2 catalysts, the NiO particles are highly concentrated, dense, and stacked on the HA surface, especially for samples with high NiO loads (15Ni/HA). This has the ability to block small-diameter pores, reducing the CO_2 adsorption base centers of the support. Meanwhile, NiO with a smaller size is more uniformly distributed on the HA surface for CeO_2-modified catalysts. This demonstrated that CeO_2 promoter increased the NiO dispersion and limited their agglomeration. This result is consistent with the TEM images of the catalysts in Figure 5.

The isotherms of the support and the typical samples, 10Ni/HA and 10Ni6Ce/HA, belong to form IV with hysteresis rings corresponding to the H3 class of the IUPAC classification[34] (Figure 6a). The presence of a medium pore structure, which is represented by type IV isotherms, is favorable for CO_2 adsorption as well as transport reactants and intermediates during the reaction.[35] Because adsorption and desorption are irreversible, hysteresis rings appear in the isotherms. They represent intergranular porosity and indirectly reflect grain size. The H3 hysteresis loop of 10Ni/HA occurs at a relative pressure of 0.3−0.9, while the H3 hysteresis ring of 10Ni6Ce/HA appears at a relatively higher pressure (0.6−0.9), indicating that the particle size of 10Ni6Ce/HA is smaller than that of 10Ni/HA.[36] Besides, the slope of the hysteresis loop of 10Ni6Ce/HA sample is higher than that of 10Ni/HA, demonstrating the larger pore size of 10Ni6Ce/HA.[37] The isotherms of both samples show no capillary condensation at low pressures (0.1−0.3), indicating that HA does not have a porous capillary structure. The pore size distribution curves (Figure 6b) show that the pore size distribution in both samples is in the range of 10−60 Å, which is typical for medium pore materials. The maximum pore size distribution of 10Ni/HA catalyst is 23.6 Å and that of 10Ni6Ce/HA sample is 23.2 Å. The BET parameters of the samples are presented in Table 1. Obviously, the pore diameters of the catalysts are suitable for CO_2 (d_{CO_2} = 0.33 nm) and H_2

Table 1. BET Surface (S_{BET}), Pore Diameter (d_{pore}), and Pore Volume (V_{pore}) of Catalysts

catalysts	S_{BET} [a] (m^2 g^{-1})	d_{pore} [a] (Å)	V_{pore} [a] (cm^3 g^{-1})	d_{NiO} [b] (nm)	H_c [c] (mmol g^{-1})
HA	13.8	24.8	0.018		
10Ni/HA	15.6	23.6	0.019	24.7	0.334
10Ni6Ce/HA	19.8	23.2	0.024	20.5	0.406

[a]BET surface (S_{BET}), average pore diameter (d_{pore}), and total pore volume (V_{pore}) were obtained from N_2 adsorption isotherm analysis. [b]Average crystalline size of NiO at 2θ = 43.3° (d_{NiO}) was estimated from XRD patterns using the Scherrer equation. [c]The H_2 consumption for the reduction of samples (H_c) was obtained from H_2-TPR results.

https://doi.org/10.1021/acsomega.2c04621
ACS Omega 2022, 7, 36623−36633

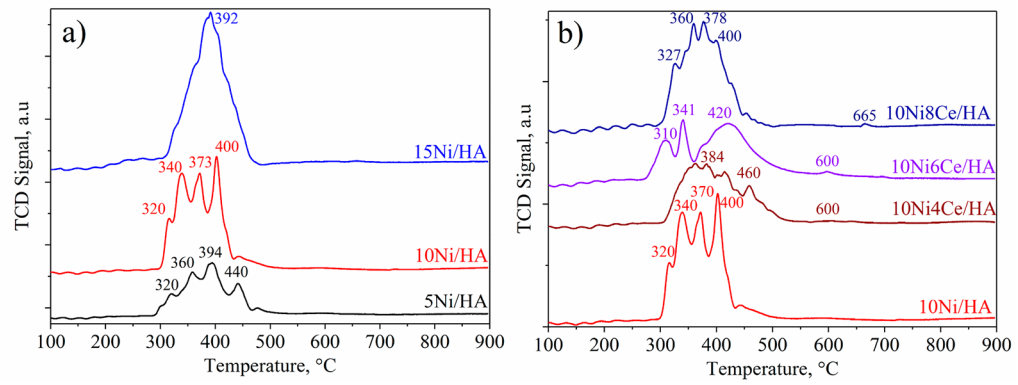

Figure 7. H_2-TPR profiles of catalysts: (a) Ni/HA and (b) Ni/HA-doped ceria.

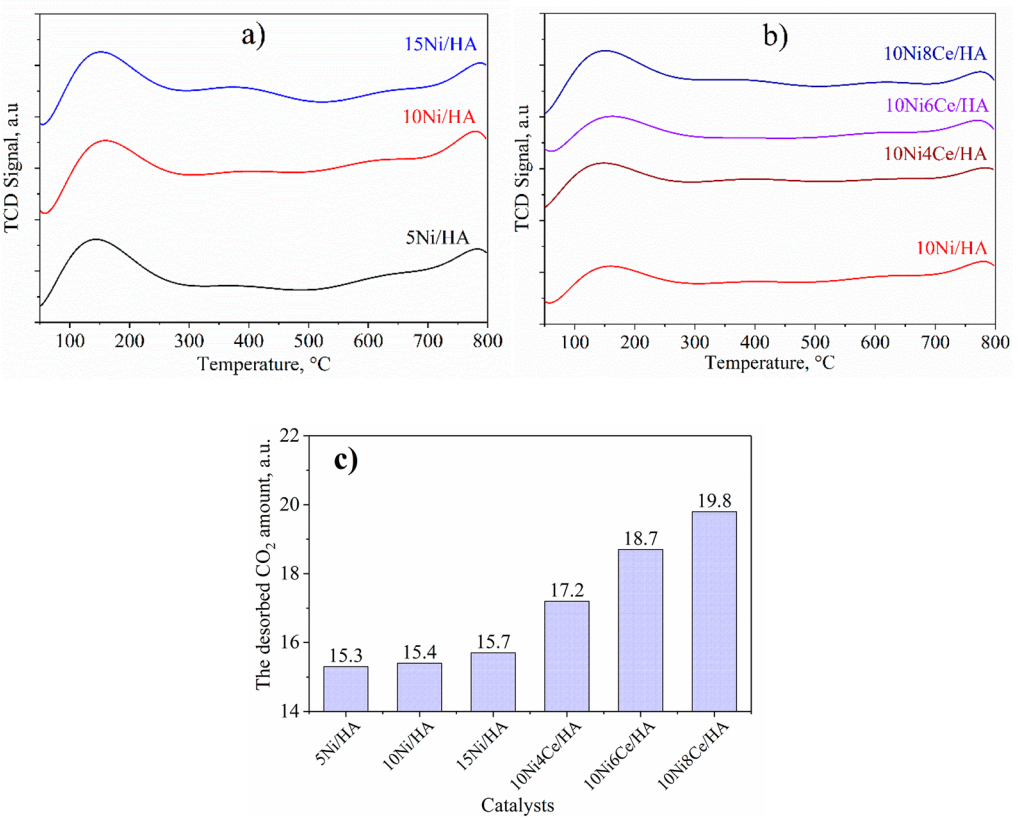

Figure 8. CO_2-TPD profiles of (a) *x*Ni/HA and (b) 10Ni/HA-doped CeO_2 catalysts, and (c) the desorbed CO_2 amount of samples.

molecules (d_{H_2} = 0.29 nm) to penetrate into the catalytic structure and perform the reaction functions.

The H_2-TPR spectra of the Ni/HA catalysts with different nickel contents (Figure 7a) show that increasing the nickel loading extends the area of the reduction peaks in the temperature range of 300−450 °C. At reduction peak temperatures of 320−360 °C, the TPR profiles of 5Ni/HA and 10Ni/HA catalysts has two characteristic peaks, corresponding to the reduction of Ni_2O_3 particles (Ni^{3+}) and NiO particles (Ni^{2+}) to Ni^0.[38] However, on the Ni/HA catalyst with higher nickel content (15Ni/HA), these reduction peaks are shifted to a higher temperature region, indicating the presence of larger-sized Ni_2O_3 and NiO particles.[39] In addition, the reduction peaks at higher temperatures are attributed to the Ni^{2+} reduction in the support structure and interact closely with them. According to some previous studies, the components that closely interact with NiO in HA were identified, including Ca^{2+} and β-TCP.[21,40−42] Among the catalysts, it can be found that 10Ni/HA is the easiest to reduce because it has a lower reduction temperature region than the others, with a complete reduction temperature of approximately 400 °C. This is also why it becomes more active during the methanation process. The H_2-TPR profiles of the ceria-doped catalysts (Figure 7b) also show characteristic peaks corresponding to the same temperature regions as the unmodified catalysts. However, these catalysts' reduction temperatures are lower than those of the unmodified ones, indicating better metal phase dispersion because CeO_2 reduces the weakening of the NiO−support interaction and increases the ability to disperse NiO on the HA surface. Besides that, Figure 7b also shows that the ceria-doped catalysts have weak reduction signals above 600 °C; these reduction signals belong

https://doi.org/10.1021/acsomega.2c04621
ACS Omega 2022, 7, 36623−36633

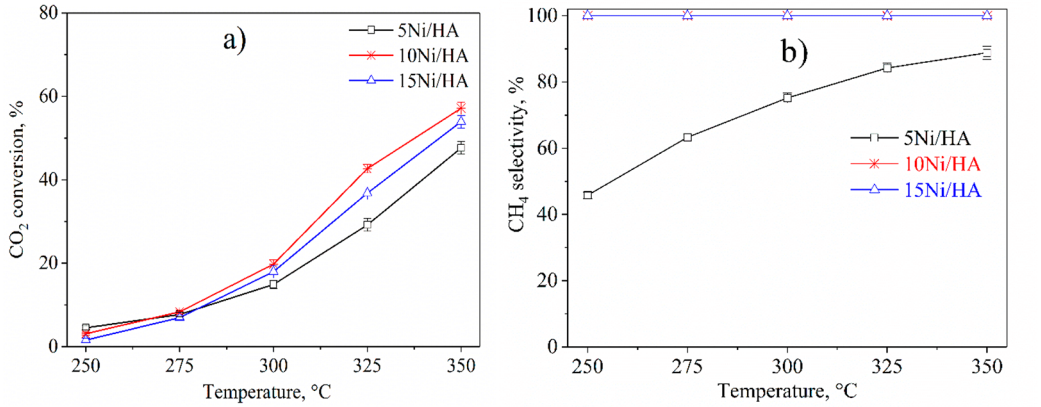

Figure 9. Activity of Ni/HA catalysts reduced at 450 °C for 2 h in CO_2 methanation with varying nickel contents: (a) CO_2 conversion and (b) CH_4 selectivity.

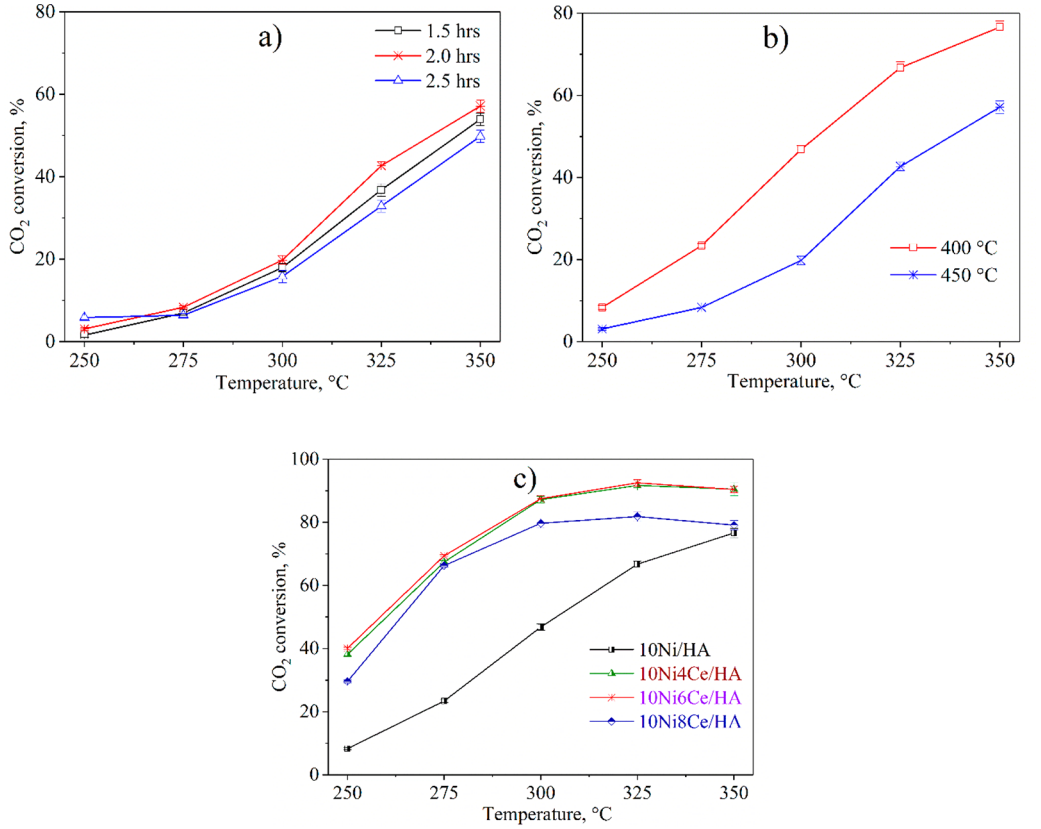

Figure 10. Activity of Ni/HA catalysts: (a) catalysts reduced at 450 °C for different durations, (b) catalysts reduced at different temperatures for 2 h, and (c) ceria-doped catalysts reduced at 400 °C for 2 h.

to the reduction process of the phases of NiO−CeO_2 interaction or surface CeO_2 in the doped catalysts.[43] The content of the CeO_2 doping is low (4−8%), so the reduction signal is not high. When compared to other catalysts, the maximum reduction peaks of 10Ni6Ce/HA are in the lowest temperature region.

The CO_2-TPD technique was used to investigate the absorption property of CO_2 reactant on the catalyst surface, which is a significant factor that may decide the activity of the catalyst. The CO_2-TPD plot of Ni/HA samples (Figure 8a) shows the appearance of two desorption peaks in the temperature regions of 80−250 °C and 650−800 °C. The broad CO_2 adsorption peak with high intensity at the temperature range of 80−250 °C indicates that the catalyst is primarily composed of weak and medium base sites. They are often assigned to the weakly active site on the surface OH, related to the bicarbonate appearance when CO_2 adsorbs on the base centers.[35] Besides, there is no adsorption peak at temperature below 80 °C, indicating that there is no physical adsorption.[44] Furthermore, the appearance of low-density adsorption peaks at higher temperatures, between 650 and 800 °C, is typical for strong base sites. These sites, according to previous reports,[21,45] mainly consist of surface OH− species that interact strongly with CO molecules. Basicity increases the CO_2 adsorption capacity, but a strong base makes CO_2 absorption difficult CO_2 that is strongly adsorbed CO_2 can

https://doi.org/10.1021/acsomega.2c04621
ACS Omega 2022, 7, 36623−36633

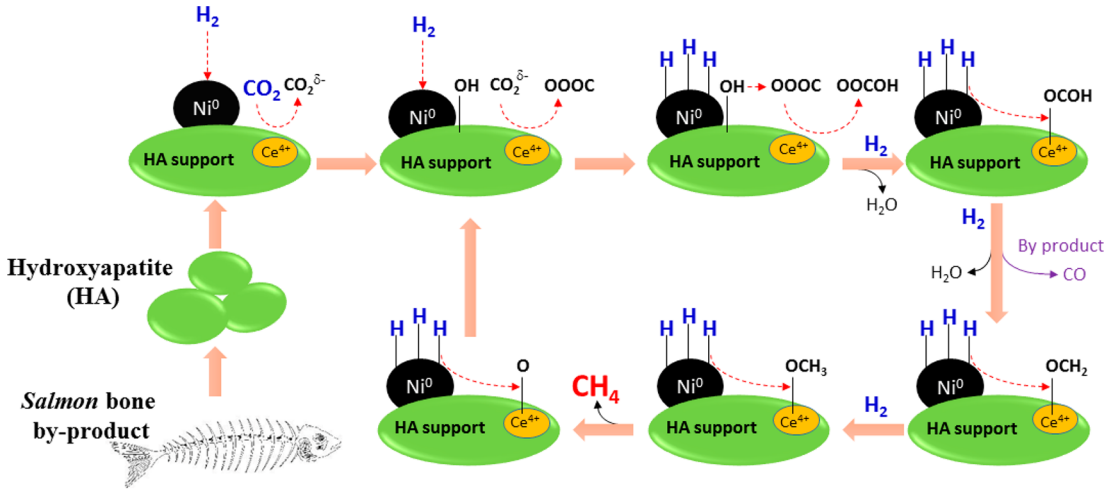

Figure 11. Schematic representation of CO_2 methanation on ceria-doped Ni/HA nanocatalyst.

inhibit CH_4 formation.[46] On the other hand, the presence of weak and medium base centers with high density is attributed to the Ca^{2+} composition of HA. When increasing, the addition of CeO_2 also increased the CO_2 adsorption capacity (Figure 8b). The addition of CeO_2 also increased the medium and weak base peaks (Figure 8b). Besides, when compared to the unmodified catalysts, the density of strong base sites was significantly reduced. As a result, weak and moderate base sites will be one of the desirable properties of a Ni catalyst for CH_4 production from CO_2. Pan et al.[47] discovered that CO_2 adsorbed at weak and moderate bases converts to monodentate carbonates and formate salts, which then combine to form CH_4. In contrast, CO_2 adsorbed at strong base sites can only form monocarbonate salts because the strong base sites impede further hydrogenation. Yan et al.[48] also suggested that increasing the weak and medium bases would improve the catalytic activity in CO_2 methanation. The overall view from the CO_2-TPD results is that the ceria doping improved the CO_2 adsorption capacity, leading to an increase in the catalytic base sites, as measured by the area of CO_2 desorbed (Figure 8c). It shows that ceria-doped 10Ni/HA catalysts have apparently higher density of base sites compared with the undoped samples.

3.2. Catalytic Activity of Studied Catalysts. The CO_2 conversion and CH_4 selectivity in the CO_2 methanation of Ni/HA catalysts with different Ni loadings reduced at 450 °C for 2 h are shown in Figure 9. It can be seen that the CO_2 conversion for the catalysts increases when the temperature is raised from 250 to 350 °C (Figure 9a). In a reaction temperature range of 250−275 °C, the catalyst activity was not different. But, in a temperature range of 300−350 °C, there is a significant difference, where the catalytic activity in terms of CO_2 conversion is arranged in the following order: 10Ni/HA > 5Ni/HA > 15Ni/HA. Figure 9b shows the outcomes and plots CO_2 conversions and CH_4 selectivities as a function of reaction temperature. The catalytic results showed that the CO_2 conversion and CH_4 selectivity increased with increasing Ni content from 5 to 10 wt %. Increasing in nickel loading higher than 10 wt % decreased the CO_2 conversion, due to decreasing the nickel dispersion as a result of bigger crystallite size as reported in Figure 2. At 350 °C, the CH_4 selectivity for the 5Ni/HA sample was around 80%, indicating that CO_2 was mainly reduced to CO instead of CH_4, by the reverse water gas shift reaction ($CO_2 + H_2 \rightarrow CO + H_2O$). For 10Ni/HA and 15Ni/HA catalysts, the CH_4 selectivity reached approximately 98% in the reaction temperature range of 250−350 °C. This implies that both of these samples have significantly larger working sites than the 5Ni/HA sample, where the catalyst exhibits high activity and selectivity, and similar results have been previously reported.[11,49] In summary, the 10Ni/HA sample exhibited higher activity than others. These results are quite consistent with all the characteristics of the catalysts.

Du et al.[11] reported that increasing the reduction time mainly affected the degree of reduction without changing the particle size or nickel dispersion. Meanwhile, according to the authors,[50,51] the reduction temperature had a significant impact on catalyst properties, such as the reduction extent, the surface area, and the dispersion of catalysts. The activity of nickel-based catalysts in the CO_2 methanation depended on the number of active Ni sites available on the catalyst surface. The reduction process influenced the Ni crystallite's size and, consequently, the surface area of active Ni sites. As Figure 10a shows, CO_2 conversion increases with increasing catalyst reduction time from 1.5 to 2.0 h at the same temperature of 450 °C, but it decreases as the catalyst reduction time increases continuously up to 2.5 h. Meanwhile, when the reduction temperature increased from 400 to 450 °C with the same suitable duration of 2 h, the CO_2 conversion decreased significantly (Figure 10b). This can be explained by the number of active nickel sites on the catalyst surface decreasing as the reduction temperature increased. But it is believed that a drop in reduction temperature results in larger nickel metal particles and their dispersion on lower supports,[52] resulting in decreased catalytic activity. Similar to the low reduction temperature, a lower number of metallic nickel sites were formed with the short reduction time, so the activity of the catalyst reduced for 1.5 h was lower than the one reduced for 2.0 h. However, in the case of a longer reduction time (2.5 h), nickel metallic particles grow up,[53] reducing the dispersion of active sites and catalytic activity. The results also revealed that the CH_4 selectivity of the catalysts activated at various times was always greater than 98%. As a result, the ideal reduction condition is 400 °C for 2.0 h.

The activity of ceria-modified catalysts reduced at the ideal condition of 400 °C for 2.0 h (Figure 10c) shows that in the temperature range of 250−350 °C, CO_2 conversion of ceria-doped samples was significantly higher than that of the undoped sample. This can be explained by the fact that the

https://doi.org/10.1021/acsomega.2c04621
ACS Omega 2022, 7, 36623−36633

Table 2. Comparison of Activity of Different Nickel-Based Catalysts in CO_2 Methanation Using a 1:4 CO_2:H_2 Molar Ratio[a]

		operating conditions							
catalysts	wt % Ni	WGHSV (mL/(g h))	T (°C)	C_{CO_2} (mol %)	X_{CO_2} (%)	S_{CH_4} (%)	H (mol CO_2/(mol Ni h)	Y (mol CH_4/(mol Ni h)	refs
10NiHA	10	12 000	325	3	76.6	98.0	8.0	7.8	this work
10Ni6CeHA	10	12 000	325	3	92.5	100	9.7	9.7	this work
	10	15 000	325	10	68.3	100	29.7	29.7	this work
	10	15 000	350	10	78.4	100	34.1	34.1	this work
10Ni4Ca/SiO_2	10	15 000	350	10	64.9	98.6	28.2	27.9	57
20NiAl-LDH	20	2400	350	18.75	75.1	95.0	4.9	4.7	58
20Ni3Fe/Al_2O_3	20	13 400	350	10	82.0	99.0	15.9	15.8	59
10Ni/Pr_2O_3- CeO_2	10	25 000	350	10	54.5	100	39.5	39.5	60
10Ni/Sm_2O_3- CeO_2	10	25 000	350	10	44.9	100	32.6	32.6	60
10Ni/MgO-CeO_2	10	25 000	350	10	43.2	100	31.3	31.3	60
20Ni/SiO_2	20	10 000	400	19	54.0	89.0	14.9	13.2	61

[a]H, CO_2 conversion efficiency calculated per Ni mole, mol CO_2/(mol Ni h); Y, CH_4 yield calculated per Ni mole, mol CH_4/(mol Ni h).

ceria-modified catalyst has a slight increase in specific surface area, which helps to increase dispersion, reduce the size of the nickel phase (Table 1), and at the same time increase the adsorption of CO_2 on the catalytic surface (Figure 8b, c). The 10Ni6Ce/HA sample had the highest activity, with CO_2 conversion reaching 92.5% at 325 °C with the CH_4 selectivity of approximately 100%. According to previous research,[54] ceria is a typical n-type semiconductor that can act as a structural and electronic promoter to promote the dispersion of Ni metal on the support and change its properties through metal-assisted interactions. In addition, ceria can be reduced to Ce_2O_3 in hydrogen-rich gases.[55] Thus, a large amount of electron-rich holes can be generated, which is favorable for CO_2 adsorption. Furthermore, holes quickly release free electrons and move from CeO_2 across the Ni−CeO_2 interface to the Ni^0 sites, thereby increasing the electron density d of the Ni atom. The electron-rich property of the Ni atom inhibits the CH_4 cracking, which is the reverse reaction of CO_2 methanation. Therefore, the reaction rate can be greatly improved by adsorbing and activating the carbon−oxygen bond, as well as inhibiting the reverse CH_4 decomposition reaction. However, when the CeO_2 content exceeds the optimal value, it also prevents NiO reduction due to the coverage of CeO_2 species on the catalyst surface, leading to a decrease in catalytic activity. A schematic of CO_2 methanation on ceria-doped nickel nanocatalyst supported on hydroxyapatite from Salmon bone could be represented in Figure 11.

In order to provide insight into the suitability of 10Ni6Ce/HA catalyst, we compared its performance with those of different Ni catalysts[56−61] (Table 2). As can be seen, a variety of supports have been examined, including SiO_2, Al_2O_3, Pr_2O_3−CeO_2, Sm_2O_3−CeO_2, and MgO−CeO_2. In most cases, the contents of the Ni active site were higher than 10 wt %. It may be concluded that although the 10Ni6Ce/HA catalyst in this study contains relatively low Ni loading (10 wt %), it can compete with these reference formulations advantageously. Especially, it exhibits highlights activity superiority when compared with Ni-based catalysts supported on Ca-modified SiO_2;[57] and approximately compared with 10Ni/CeO_2 catalyst modified Pr_2O_3, Sm_2O_3, and MgO,[60] assayed under similar conditions. Moreover, it is clear that the promoting effect of CeO_2 on the activity of Ni catalyst is more pronounced for hydroxyapatite-based materials, suggesting the suitability of green support for the CO_2 methanation. It should be stressed that the improved structural, chemical, and catalytic properties of Ni-based catalysts supported on hydroxyapatite-derived *Salmon* bone byproduct represent an advantageous alternative to traditional fundamental catalysts.

4. CONCLUSION

Highly active Ni/HA and CeO_2-doped Ni/HA catalysts in the CO_2 methanation were synthesized via a simple and eco-friendly method. Because of the presence of Ca^{2+} ions in the HA structure, CO_2 adsorption was improved, leading to enhanced catalytic activity. Furthermore, the addition of CeO_2 to the Ni/HA catalyst improves NiO dispersion on the HA surface, resulting in smaller NiO crystals, enhanced NiO reduction level as well as CO_2 adsorption capacity, and improved catalytic activity in the low temperature. The 10Ni/HA catalyst-doped 6.0 wt % CeO_2 had the highest catalytic performance, with a CO_2 conversion of 92.5% and a CH_4 selectivity of approximately 100% at 325 °C. Hence, the use of CeO_2-doped Ni/HA catalyst is one of the most promising approaches in designing efficient catalyst structures toward the development of effective CO_2 hydrogenation to CH_4 fuel on an industrial scale.

■ ASSOCIATED CONTENT

Data Availability Statement

The data used to support the findings of this study are included within the article.

■ AUTHOR INFORMATION

Corresponding Authors

Tri Nguyen − *Institute of Chemical Technology, Vietnam Academy of Science and Technology, Ho Chi Minh City, Vietnam;* orcid.org/0000-0001-9486-5096; Email: ntri@ict.vast.vn

Ha Ky Phuong Huynh − *Faculty of Chemical Engineering, Ho Chi Minh City University of Technology (HCMUT), Ho Chi Minh City, Vietnam; Vietnam National University Ho Chi Minh City, Ho Chi Minh City, Vietnam;* orcid.org/0000-0002-0504-2678; Email: hkpha@hcmut.edu.vn

Authors

Thi Thuy Van Nguyen − *Institute of Chemical Technology, Vietnam Academy of Science and Technology, Ho Chi Minh City, Vietnam;* orcid.org/0000-0002-1002-9814

https://doi.org/10.1021/acsomega.2c04621
ACS Omega 2022, 7, 36623−36633

Nguyen Phung Anh − *Institute of Chemical Technology, Vietnam Academy of Science and Technology, Ho Chi Minh City, Vietnam*
Thanh Gia-Thien Ho − *Institute of Chemical Technology, Vietnam Academy of Science and Technology, Ho Chi Minh City, Vietnam*
Thi Thuy Phuong Pham − *Institute of Chemical Technology, Vietnam Academy of Science and Technology, Ho Chi Minh City, Vietnam*
Phuc Hoang Duy Nguyen − *Institute of Chemical Technology, Vietnam Academy of Science and Technology, Ho Chi Minh City, Vietnam*
Ba Long Do − *Institute of Chemical Technology, Vietnam Academy of Science and Technology, Ho Chi Minh City, Vietnam*

Complete contact information is available at: https://pubs.acs.org/10.1021/acsomega.2c04621

Notes

The authors declare no competing financial interest.

■ ACKNOWLEDGMENTS

This study is supported by the Vietnam Academy of Science and Technology under the NCXS02.02/22-23 project.

■ REFERENCES

(1) Mead, I.*International Energy Outlook 2017*; U.S. Energy Information Administration: Washington. D.C., 2017.
(2) Mardani, A.; Streimikiene, D.; Cavallaro, F.; Loganathan, N.; Khoshnoudi, M. Carbon dioxide (CO_2) emissions and economic growth: A systematic review of two decades of research from 1995 to 2017. *Sci. Total Environ.* **2019**, *649*, 31−49.
(3) Takht Ravanchi, M.; Sahebdelfar, S. Catalytic conversions of CO_2 to help mitigate climate change: Recent process developments. *Process Saf. Environ. Prot* **2021**, *145*, 172−194.
(4) Peters, G. P.; Andrew, R. M.; Canadell, J. G.; Friedlingstein, P.; Jackson, R. B.; Korsbakken, J. I.; Le Quéré, C.; Peregon, A. Carbon dioxide emissions continue to grow amidst slowly emerging climate policies. *Nat. Clim. Chang* **2020**, *10* (1), 3−6.
(5) Asghar, U.; Rafiq, S.; Anwar, A.; Iqbal, T.; Ahmed, A.; Jamil, F.; Khurram, M. S.; Akbar, M. M.; Farooq, A.; Shah, N. S.; Park, Y.-K. Review on the progress in emission control technologies for the abatement of CO_2, SO_x and NO_x from fuel combustion. *J. Environ. Chem. Eng.* **2021**, *9* (5), 106064.
(6) Gielen, D.; Boshell, F.; Saygin, D.; Bazilian, M. D.; Wagner, N.; Gorini, R. The role of renewable energy in the global energy transformation. *Energy Strategy Rev.* **2019**, *24*, 38−50.
(7) Santos, D. B. L.; Noronha, F. B.; Hori, C. E. Bi-reforming of methane for hydrogen production using $LaNiO_3/Ce_xZr_{1-x}O_2$ as precursor material. *Int. J. Hydrog. Energy* **2020**, *45* (27), 13947−13959.
(8) Ashok, J.; Pati, S.; Hongmanorom, P.; Tianxi, Z.; Junmei, C.; Kawi, S. A review of recent catalyst advances in CO_2 methanation processes. *Catal. Today* **2020**, *356*, 471−489.
(9) Le, T. A.; Kim, M. S.; Lee, S. H.; Kim, T. W.; Park, E. D. CO and CO_2 methanation over supported Ni catalysts. *Catal. Today* **2017**, *293*, 89−96.
(10) Kester, K. B.; Zagli, E.; Falconer, J. L. Methanation of carbon monoxide and carbon dioxide on Ni/Al_2O_3 catalysts: effects of nickel loading. *Appl. Catal* **1986**, *22* (2), 311−319.
(11) Du, G.; Lim, S.; Yang, Y.; Wang, C.; Pfefferle, L.; Haller, G. L. Methanation of carbon dioxide on Ni-incorporated MCM-41 catalysts: The influence of catalyst pretreatment and study of steady-state reaction. *J. Catal.* **2007**, *249* (2), 370−379.
(12) Frontera, P.; Macario, A.; Ferraro, M.; Antonucci, P. Supported catalysts for CO_2 methanation: a review. *Catalysts* **2017**, *7* (2), 59.
(13) Wai, M. H.; Ashok, J.; Dewangan, N.; Das, S.; Xi, S.; Borgna, A.; Kawi, S. Influence of surface formate species on methane selectivity for carbon dioxide methanation over nickel hydroxyapatite catalyst. *ChemCatChem.* **2020**, *12* (24), 6410−6419.
(14) Kay, M. I.; Young, R. A.; Posner, A. S. Crystal structure of hydroxyapatite. *Nature* **1964**, *204* (4963), 1050−1052.
(15) Kaneda, K.; Mizugaki, T. Development of concerto metal catalysts using apatite compounds for green organic syntheses. *Energy Environ. Sci.* **2009**, *2* (6), 655−673.
(16) Cheng, Z. H.; Yasukawa, A.; Kandori, K.; Ishikawa, T. FTIR study of adsorption of CO_2 on nonstoichiometric calcium hydroxyapatite. *Langmuir* **1998**, *14* (23), 6681−6686.
(17) Cui, Q.; Chao, S.; Bai, Z.; Yan, H.; Wang, K.; Yang, L. Based on a new support for synthesis of highly efficient palladium/hydroxyapatite catalyst for ethanol electrooxidation. *Electrochim. Acta* **2014**, *132*, 31−36.
(18) Le Hoang, T. T. T.; Insin, N.; Sukpirom, N. Catalytic activity of silver nanoparticles anchored on layered double hydroxides and hydroxyapatite. *Inorg. Chem. Commun.* **2020**, *121*, 108199.
(19) Oh, S. C.; Wu, Y.; Tran, D. T.; Lee, I. C.; Lei, Y.; Liu, D. Influences of cation and anion substitutions on oxidative coupling of methane over hydroxyapatite catalysts. *Fuel* **2016**, *167*, 208−217.
(20) Petit, S.; Thomas, C.; Millot, Y.; Averseng, F.; Brouri, D.; Krafft, J. m.; Dzwigaj, S.; Rousse, G.; Laberty-Robert, C.; Costentin, G. Synergistic effect between $Ca_4V_4O_{14}$ and vanadium-substituted hydroxyapatite in the oxidative dehydrogenation of propane. *ChemCatChem.* **2021**, *13* (18), 3995−4009.
(21) Boukha, Z.; Yeste, M. P.; Cauqui, M. Á.; González-Velasco, J. R. Influence of Ca/P ratio on the catalytic performance of Ni/hydroxyapatite samples in dry reforming of methane. *Appl. Catal. A: Gen* **2019**, *580*, 34−45.
(22) Iriarte-Velasco, U.; Ayastuy, J. L.; Boukha, Z.; Bravo, R.; Gutierrez-Ortiz, M. Á. Transition metals supported on bone-derived hydroxyapatite as potential catalysts for the Water-Gas Shift reaction. *Renew. Energy* **2018**, *115*, 641−648.
(23) Li, X.; Wang, Y.; Wei, X.; Zhao, Y. Effect of Na promoter on the catalytic performance of Pd-Cu/hydroxyapatite catalyst for room-temperature CO oxidation. *Mol. Catal* **2020**, *491*, 111002.
(24) Fechete, I.; Vedrine, J. C. Nanoporous materials as new engineered catalysts for the synthesis of green fuels. *Molecules* **2015**, *20* (4), 5638−5666.
(25) Corthals, S.; Van Nederkassel, J.; Geboers, J.; De Winne, H.; Van Noyen, J.; Moens, B.; Sels, B.; Jacobs, P. Influence of composition of $MgAl_2O_4$ supported $NiCeO_2ZrO_2$ catalysts on coke formation and catalyst stability for dry reforming of methane. *Catal. Today* **2008**, *138* (1−2), 28−32.
(26) Aneggi, E.; De Leitenburg, C.; Dolcetti, G.; Trovarelli, A. Promotional effect of rare earths and transition metals in the combustion of diesel soot over CeO_2 and CeO_2-ZrO_2. *Catal. Today* **2006**, *114* (1), 40−47.
(27) Bradford, M. C.; Vannice, M. A. The role of metal-support interactions in CO_2 reforming of CH_4. *Catal. Today* **1999**, *50* (1), 87−96.
(28) Kambolis, A.; Matralis, H.; Trovarelli, A.; Papadopoulou, C. Ni/CeO_2-ZrO_2 catalysts for the dry reforming of methane. *Appl. Catal. A: Gen* **2010**, *377* (1−2), 16−26.
(29) Li, D.; Zeng, L.; Li, X.; Wang, X.; Ma, H.; Assabumrungrat, S.; Gong, J. Ceria-promoted Ni/SBA-15 catalysts for ethanol steam reforming with enhanced activity and resistance to deactivation. *Appl. Catal. B: Environ* **2015**, *176*, 532−541.
(30) Xavier, K. O.; Sreekala, R.; Rashid, K. K. A.; Yusuff, K. K. M.; Sen, B. Doping effects of cerium oxide on Ni/Al_2O_3 catalysts for methanation. *Catal. Today* **1999**, *49* (1−3), 17−21.
(31) Tri, N.; Trang, T. N.; Trinh, N. H.; Tung, L. T.; Van, N. T.; Anh, N. P.; Tan, N. D.; No, N. T.; Ha, H. K. Hydrothermal and calcination regimes and characteristics of nanohydroxyapatite synthesized from *Salmon* bones. *J. Biochem. Technol.* **2020**, *11* (2), 82−87.

(32) Tamai, M.; Isama, K.; Nakaoka, R.; Tsuchiya, T. Synthesis of a novel b-tricalcium phosphate/hydroxyapatite biphasic calcium phosphate containing niobium ions and evaluation of its osteogenic properties. *Int. J. Artif. Organs* **2007**, *10* (1), 22−28.
(33) Huang, A.; Dai, H.; Wu, X.; Zhao, Z.; Wu, Y. Synthesis and characterization of mesoporous hydroxyapatite powder by micro-emulsion technique. *J. Mater. Res. Technol.* **2019**, *8* (3), 3158−3166.
(34) Sing, K. S. W. Reporting physisorption data for gas/solid systems with special reference to the determination of surface area and porosity (Recommendations 1984). *Pure Appl. Chem.* **1985**, *57* (4), 603−619.
(35) Jia, X.; Zhang, X.; Rui, N.; Hu, X.; Liu, C.-j. Structural effect of Ni/ZrO_2 catalyst on CO_2 methanation with enhanced activity. *Appl. Catal. B: Environ* **2019**, *244*, 159−169.
(36) Aziz, M. A. A.; Jalil, A. A.; Triwahyono, S.; Mukti, R. R.; Taufiq-Yap, Y. H.; Sazegar, M. R. Highly active Ni-promoted mesostructured silica nanoparticles for CO_2 methanation. *Appl. Catal. B: Environ* **2014**, *147*, 359−368.
(37) El Shafei, G. M. S.; Moussa, N. A. Adsorption of some essential amino acids on hydroxyapatite. *J. Colloid Interface Sci.* **2001**, *238* (1), 160−166.
(38) Sidik, S.; Triwahyono, S.; Jalil, A.; Aziz, M.; Fatah, N.; Teh, L. Tailoring the properties of electrolyzed Ni/mesostructured silica nanoparticles (MSN) via different Ni-loading methods for CO_2 reforming of CH_4. *J. CO_2 Util* **2016**, *13*, 71−80.
(39) de Freitas Silva, T.; Dias, J. A. C.; Maciel, C. G.; Assaf, J. M. Ni/Al_2O_3 catalysts: effects of the promoters Ce, La and Zr on the methane steam and oxidative reforming reactions. *Catal. Sci. Technol.* **2013**, *3* (3), 635−643.
(40) Li, B.; Yuan, X.; Li, B.; Wang, X. Impact of pore structure on hydroxyapatite supported nickel catalysts (Ni/HAP) for dry reforming of methane. *Fuel Process. Technol.* **2020**, *202*, 106359.
(41) Boukha, Z.; Kacimi, M.; Pereira, M. F. R.; Faria, J. L.; Figueiredo, J. L.; Ziyad, M. Methane dry reforming on Ni loaded hydroxyapatite and fluoroapatite. *Appl. Catal. A: Gen* **2007**, *317* (2), 299−309.
(42) Jun, J. H.; Lee, T.-J.; Lim, T. H.; Nam, S.-W.; Hong, S.-A.; Yoon, K. J. Nickel-calcium phosphate/hydroxyapatite catalysts for partial oxidation of methane to syngas: characterization and activation. *J. Catal.* **2004**, *221* (1), 178−190.
(43) Alvarez-Galvan, C.; Martínez, J. L.; Capel-Sanchez, M.; Pascual, L.; Alonso, J. A. Magnetic properties of efficient catalysts based on La-doped ceria-supported nickel nanoparticles for rWGS reaction. Influence of Ni loading. *Adv. Sustain. Syst* **2021**, *5* (11), 2100029.
(44) Rui, N.; Wang, Z.; Sun, K.; Ye, J.; Ge, Q.; Liu, C.-j. CO_2 hydrogenation to methanol over Pd/In_2O_3: effects of Pd and oxygen vacancy. *Appl. Catal. B: Environ* **2017**, *218*, 488−497.
(45) Boukha, Z.; Gil-Calvo, M.; de Rivas, B.; Gonzalez-Velasco, J. R.; Gutierrez-Ortiz, J. I.; López-Fonseca, R. Behaviour of Rh supported on hydroxyapatite catalysts in partial oxidation and steam reforming of methane: on the role of the speciation of the Rh particles. *Appl. Catal. A: Gen* **2018**, *556*, 191−203.
(46) Muroyama, H.; Tsuda, Y.; Asakoshi, T.; Masitah, H.; Okanishi, T.; Matsui, T.; Eguchi, K. Carbon dioxide methanation over Ni catalysts supported on various metal oxides. *J. Catal.* **2016**, *343*, 178−184.
(47) Pan, Q.; Peng, J.; Sun, T.; Wang, S.; Wang, S. Insight into the reaction route of CO_2 methanation: Promotion effect of medium basic sites. *Catal. Commun.* **2014**, *45*, 74−78.
(48) Yan, Y.; Dai, Y.; Yang, Y.; Lapkin, A. A. Improved stability of Y_2O_3 supported Ni catalysts for CO_2 methanation by precursor-determined metal-support interaction. *Appl. Catal. B: Environ* **2018**, *237*, 504−512.
(49) Ilsemann, J.; Sonström, A.; Gesing, T. M.; Anwander, R.; Bäumer, M. Highly active Sm_2O_3-Ni xerogel catalysts for CO_2 methanation. *ChemCatChem.* **2019**, *11* (6), 1732−1741.
(50) de Leitenburg, C.; Trovarelli, A.; Kašpar, J. A temperature-programmed and transient kinetic study of CO_2 activation and methanation over CeO_2 supported noble metals. *J. Catal.* **1997**, *166* (1), 98−107.
(51) Bartholomew, C. H.; Farrauto, R. J. Chemistry of nickel-alumina catalysts. *J. Catal.* **1976**, *45* (1), 41−53.
(52) Manukyan, K. V.; Avetisyan, A. G.; Shuck, C. E.; Chatilyan, H. A.; Rouvimov, S.; Kharatyan, S. L.; Mukasyan, A. S. Nickel oxide reduction by hydrogen: kinetics and structural transformations. *J. Phys. Chem. C* **2015**, *119* (28), 16131−16138.
(53) Hidayat, T.; Rhamdhani, M.; Jak, E.; Hayes, P. On the relationships between the kinetics and mechanisms of gaseous hydrogen reduction of solid nickel oxide. *Metall. Mater. Trans. B* **2009**, *40* (4), 474−489.
(54) Ahmed, W.; Awadallah, A. E.; Aboul-Enein, A. A. Ni/CeO_2-Al_2O_3 catalysts for methane thermo-catalytic decomposition to CO_x-free H_2 production. *Int. J. Hydrog. Energy* **2016**, *41* (41), 18484−18493.
(55) Yang, R.; Xing, C.; Lv, C.; Shi, L.; Tsubaki, N. Promotional effect of La_2O_3 and CeO_2 on Ni/γ-Al_2O_3 catalysts for CO_2 reforming of CH_4. *Appl. Catal. A: Gen* **2010**, *385* (1−2), 92−100.
(56) Garbarino, G.; Bellotti, D.; Riani, P.; Magistri, L.; Busca, G. Methanation of carbon dioxide on Ru/Al_2O_3 and Ni/Al_2O_3 catalysts at atmospheric pressure: catalysts activation, behaviour and stability. *Int. J. Hydrog. Energy* **2015**, *40* (30), 9171−9182.
(57) Guo, M.; Lu, G. The difference of roles of alkaline-earth metal oxides on silica-supported nickel catalysts for CO_2 methanation. *RSC Adv.* **2014**, *4* (102), 58171−58177.
(58) He, S.; Li, C.; Chen, H.; Su, D.; Zhang, B.; Cao, X.; Wang, B.; Wei, M.; Evans, D. G.; Duan, X. A surface defect-promoted Ni nanocatalyst with simultaneously enhanced activity and stability. *Chem. Mater.* **2013**, *25* (7), 1040−1046.
(59) Mutz, B.; Belimov, M.; Wang, W.; Sprenger, P.; Serrer, M.-A.; Wang, D.; Pfeifer, P.; Kleist, W.; Grunwaldt, J.-D. Potential of an alumina-supported Ni3Fe catalyst in the methanation of CO_2: Impact of alloy formation on activity and stability. *ACS Catal.* **2017**, *7* (10), 6802−6814.
(60) Siakavelas, G. I.; Charisiou, N. D.; AlKhoori, S.; AlKhoori, A. A.; Sebastian, V.; Hinder, S. J.; Baker, M. A.; Yentekakis, I.; Polychronopoulou, K.; Goula, M. A. Highly selective and stable nickel catalysts supported on ceria promoted with Sm_2O_3, Pr_2O_3 and MgO for the CO_2 methanation reaction. *Appl. Catal. B: Environ* **2021**, *282*, 119562.
(61) Zhu, P.; Chen, Q.; Yoneyama, Y.; Tsubaki, N. Nanoparticle modified Ni-based bimodal pore catalysts for enhanced CO_2 methanation. *RSC Adv.* **2014**, *4* (110), 64617−64624.

https://doi.org/10.1021/acsomega.2c04621
ACS Omega 2022, 7, 36623−36633